

See You Soon: Decoupled Iterative Refinement Framework for Interacting Hands Reconstruction from a Single RGB Image

Pengfei Ren^{1,2}, Chao Wen², Xiaozheng Zheng^{1,2}, Zhou Xue², Haifeng Sun¹,
Qi Qi¹, Jingyu Wang¹, Jianxin Liao¹

¹ State Key Laboratory of Networking and Switching Technology,
Beijing University of Posts and Telecommunications

² Pico IDL, ByteDance

Abstract

Reconstructing interacting hands from a single RGB image is a very challenging task. On the one hand, severe mutual occlusion and similar local appearance between two hands confuse the extraction of visual features, resulting in the misalignment of estimated hand meshes and the image. On the other hand, there are complex interaction patterns between interacting hands, which significantly increases the solution space of hand poses and increases the difficulty of network learning. In this paper, we propose a decoupled iterative refinement framework to achieve pixel-alignment hand reconstruction while efficiently modeling the spatial relationship between hands. Specifically, we define two feature spaces with different characteristics, namely 2D visual feature space and 3D joint feature space. First, we obtain joint-wise features from the visual feature map and utilize a graph convolution network and a transformer to perform intra- and inter-hand information interaction in the 3D joint feature space, respectively. Then, we project the joint features with global information back into the 2D visual feature space in an obfuscation-free manner and utilize the 2D convolution for pixel-wise enhancement. By performing multiple alternate enhancements in the two feature spaces, our method can achieve an accurate and robust reconstruction of interacting hands. Our method outperforms all existing two-hand reconstruction methods by a large margin on the InterHand2.6M dataset. Meanwhile, our method shows a strong generalization ability for in-the-wild images.

1. Introduction

3D hand reconstruction plays an important role in many applications, such as virtual reality (VR), augmented reality (AR), robotics, etc. With the emergence of large-scale datasets and deep learning, single-hand pose estimation and reconstruction [1, 2, 5–9, 19, 21, 31, 32, 34, 41, 51, 55, 56]

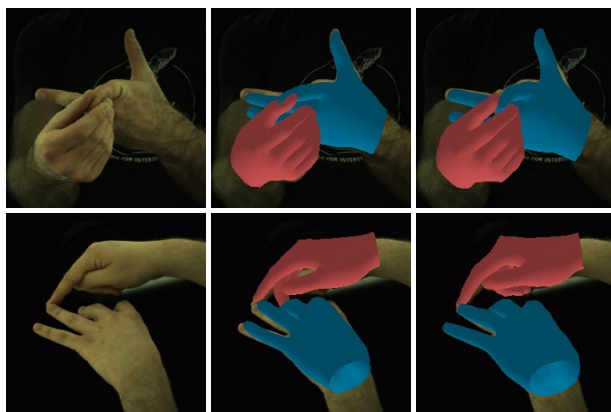


Figure 1. The first and second rows show the importance of spatial relationship modeling and mesh-image alignment, respectively. IntagHand [23] is a recently proposed SOTA interacting hands reconstruction method.

have made significant progress in the past few years. Furthermore, since two hands can express richer semantics and implement more complex operations, interacting two-hand reconstruction has received a lot of attention recently. However, previous work usually relies on depth cameras [3, 22, 35, 36, 44] or multi-camera systems [40], which greatly limits the application scenarios of these methods. In this paper, considering that RGB images are widely available, we focus on reconstructing interacting hands from a single RGB image.

Compared to the single-hand reconstruction task, reconstructing the interacting hands from a single RGB image is more challenging and far from being solved. On the one hand, severe mutual occlusion between interacting hands results in a large amount of hand area being unobservable. At the same time, the self-similar appearance brings severe ambiguity and confusion to the extraction of visual representations. Thus, self-occlusion and self-similarity tend to cause

misalignment between the estimated hand meshes and the input image. On the other hand, the interacting hands have complex spatial relationships, and the dramatic increase in the degrees of freedom of the pose solution brings difficulties to the optimization of the network.

Some methods attempt to alleviate the interference of self-occlusion and similar appearance by utilizing some visual cues such as heatmaps [49], joint-visibility [20], and part-segmentation [13]. Nonetheless, these methods ignore the tight dependency between interacting hands. In order to better capture the spatial relationship between hands, Hampali et al. [17] extract redundant node features from the visual feature map and use a transformer to perform message passing between nodes of two hands. To achieve pixel-level alignment, Li et al. [23] propose a dense attention mechanism to progressively enhance the vertex features of the hand mesh with the image features. However, dense interactions are computationally expensive and suffer from the risk of overfitting. In the field of human body reconstruction and single-hand reconstruction, some methods [25, 43, 50] attempt to densely extract vertex-wise perceptual features from image feature maps, thereby achieving mesh-image alignment. However, due to the severe self-occlusion and self-similarity of the interacting two-hand, the visual feature quality is often not reliable enough. Therefore, it is not sufficient to only adopt a unidirectional feature extraction process from the feature map to the 3D mesh space.

The core insight of our paper is to decouple pixel-level alignment and two-hand spatial relationship modeling to achieve high-precision mesh-image alignment while maintaining a reasonable two-hand spatial relationship. Specifically, our method explicitly defines two feature spaces, 2D visual feature space and 3D joint feature space, respectively. We communicate the two spaces through 2D-3D projection relationship for iterative feature enhancement. First, we compress the visual features into compact joint features and use a Graph Convolution Network (GCN) [52] and a transformer [53] to model the intra- and inter-relationships of two hands, respectively. Then, we project the enhanced joint features back to the visual feature space in an obfuscation-free way, so as to refine local visual features. Performing long-range relational modeling in joint feature space is computationally friendly and can take advantage of skeletal structure information. At the same time, joint features with global information can provide strong disambiguation clues for local visual features, alleviating the information loss caused by self-occlusion and the ambiguity caused by self-similarity.

Experiments show that our method significantly outperforms State-Of-The-Art (SOTA) methods (7.52 mm vs 8.79 mm) on the InterHand2.6M dataset [23]. At the same time, we also show the qualitative results of our method on multiple in-the-wild samples [4, 39, 45, 46], from which we can

observe that our method has a strong generalization ability.

Our contributions can be summarized as follows:

- We propose a decoupled iterative refinement framework for reconstructing interacting hands from a single RGB image. Our method achieves pixel-level mesh-image alignment while efficiently modeling the spatial relationship of the hands.
- We model the spatial relationship of the two hands through compact and semantically explicit joint nodes, which is computationally friendly and can utilize the priors of hand bone structure.
- We propose an obfuscation-free way to project joint-wise features with global information into visual feature space, which alleviates the ambiguity caused by self-similarity and lack of visual cues caused by self-occlusion.
- Our method outperforms recent SOTA methods by a large margin and shows a strong generalization ability for the in-the-wild images.

2. Related Works

2.1. Single Hand Reconstruction

Early single-hand reconstruction work relied on depth data, but with the emergence of large-scale datasets and the development of deep learning, RGB-based hand reconstruction has made great progress. Pioneering RGB-based work focus on only estimating hand pose from input [6, 19, 42, 55]. With the proposal of parametric hand models, some work [5, 30, 51, 54] attempt to reconstruct hands directly from RGB images using MANO models. However, it is challenging to predict the parameters of the hand model from a single RGB image, which leads to difficulties in network optimization and is prone to mesh-image misalignment [43]. To alleviate these problems, some works propose to use GCN [11, 14, 21] or transformer [10, 24, 25] to directly estimate the coordinates of the vertices of the hand mesh. However, reconstructing the hand without prior knowledge can easily lead to the collapse of the predicted mesh, even if these methods adopt some constraint terms to keep the generated mesh smooth. Therefore, in order to keep the estimated hand model reasonable, we adopt a parametric hand model and alleviate the mesh-image misalignment through the iterative 3D spatial relationship modeling and the 2D feature enhancement.

2.2. Interacting Hand Reconstruction

Interacting hand reconstruction is a very challenging problem. Some pioneering work [3, 22, 36] fit a parametric hand model with observed depth data by optimizing an

energy function. These methods tend to be trapped in local optima and are computationally expensive. A common approach is to train a deep neural network to predict some visual cues, such as segmentation [35, 44], pixel-mesh correspondence map [35, 46] or the dense relative depth map of the interacting hands [46], to reduce the search space of hand poses and the optimization difficulty of the energy function. However, this hybrid approach cannot be trained in an end-to-end manner and the optimization process may still fall into local minima. Recently, Smith et al. [40] propose a multi-view camera system, which can reconstruct high-fidelity interacting hand motions. However, this method requires custom-built dedicated hardware and the algorithm is time-consuming.

In recent years, with the proposal of the large-scale interacting hand dataset InterHand2.6M [33], great progress has been made in single RGB-based 3D interacting hands reconstruction. Moon et al. [33] extend the single-hand pose estimation method to the two-hand interacting scenario, which predicts the 2.5D heatmap of the two hands simultaneously. Some works improve the accuracy of the interacting hand estimation by incorporating some visual cues such as joint-visibility [20] and part-segmentation [13]. In order to reduce the mutual interference between interacting hands, Zhang et al. [49] propose to use heatmaps to make the network focus on specific regions, and Meng et al. [29] adopt an erase mechanism to convert the two-hand image into two single-hand images. However, these methods do not adequately model the dependencies between the two hands. Hampali et al. [17] adopt the transformer to model the interaction between two hands, which is robust but still hard to mitigate misalignment between the estimated hand pose and the image. Li et al. [23] progressively enhance mesh vertex features with image features while performing information interaction between two-hand meshes, which is helpful for mesh-image alignment. However, performing dense mesh-mesh and mesh-images interactions is computationally complex and prone to overfitting.

2.3. Pixel-level Alignment

Estimating pixel-aligned 3D mesh directly from a single RGB image is quite challenging, either by estimating parametric models or by directly predicting mesh vertex coordinates. Wang et al. [47] and Wen et al. [48] propose to use the camera intrinsic matrix to obtain the perceptual features of each 3D mesh vertex from the 2D image features according to the 3D-2D coordinate relationship. Further, Zhang et al. [50] and Tang et al. [43] extend this strategy to extract human body mesh and hand mesh features from visual features, respectively, in order to obtain a more accurate mesh-image alignment. In addition to sampling mesh features using coordinate relations, another way [23, 25] is to use a transformer to perform densely interaction between

image features and vertex features. However, this method is computationally expensive and relatively sensitive to self-occlusion (the correctness of the interaction relationship is affected by the quality of the feature itself). In particular, the above two methods only perform feature enhancement in the 3D vertex space, ignoring the role of the 2D feature space. Specifically, the local receptive field mechanism of 2D convolution operation provides intrinsic inductive bias, which can efficiently and effectively utilize local features for pixel-level refinement. Our method projects joint features with global information back into the 2D visual feature space, which further provides strong cues for 2D convolution to achieve more accurate pixel-level alignment.

3. Method

In this paper, we propose a decoupled iterative refinement module for interacting two-hand reconstruction from a single RGB image. As shown in Fig. 2, we adopt an encoding-decoding network structure. The encoder extracts multi-scale visual features and uses global features to estimate the initial hand meshes. During the decoding process, we progressively enhance the visual feature maps and iteratively refine the hand meshes.

3.1. Encoder and Initial Estimation

We adopt a ResNet-50 [18] pretrained on ImageNet [12] as the encoder, from which we can obtain multi-scale visual features $\{\mathbf{F}_n^{img} \in \mathbb{R}^{C_n \times H_n \times W_n}\}_{n=0}^{N-1}$, where N, C_n, H_n, W_n represent the number of visual feature scales, the channel dimension, height and width of the n -th feature map respectively. In general, direct regression of vertex coordinates can achieve higher accuracy mesh prediction [14, 21, 25, 43]. However, this method is prone to generate collapsed and unreasonable hand mesh, so the robustness is relatively poor. Therefore, we use the global features extracted by the encoder to regress the parameters of a parameterized hand model MANO [38] directly and then improve the accuracy of the initial meshes through subsequent iterative refinement. In particular, the two hands should have their own unique features, so we adopt a simple and lightweight attention module to separate the features of the two hands from the highest-level image feature map \mathbf{F}_{N-1}^{img} . Taking the left hand as an example, the left hand feature $\mathbf{F}_{left}^{img} \in \mathbb{R}^{C_{N-1}}$ can be obtained by an attention map $\mathbf{A}_{left} \in \mathbb{R}^{1 \times H_{N-1} \times W_{N-1}}$ as follow:

$$\mathbf{A}_{left} = \text{Sigmoid} \left(\text{Conv}_{left} \left(\mathbf{F}_{N-1}^{img} \right) \right), \quad (1)$$

$$\mathbf{F}_{left}^{img} = \text{AvgPool} \left(\mathbf{A}_{left} * \mathbf{F}_{N-1}^{img} \right). \quad (2)$$

Then, we estimate model parameters ($\theta_{left} \in \mathbb{R}^{62}$ and $\theta_{right} \in \mathbb{R}^{62}$) and weak perspective camera parameters

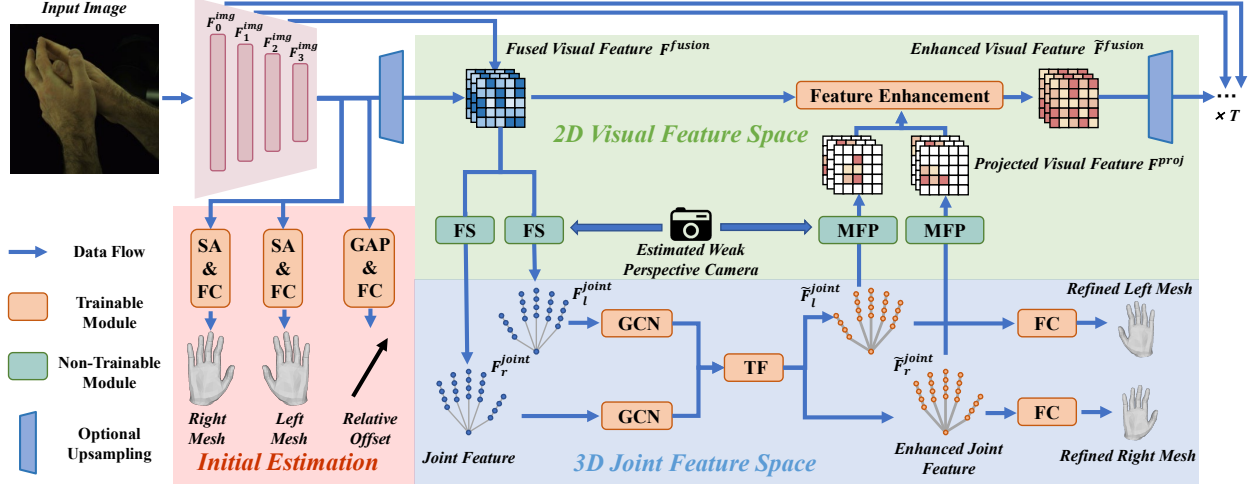


Figure 2. Our framework. We utilize the global features extracted by the encoder to predict the initial hand mesh and the relative offset of the hands. Then, the decoder gradually fuses the multi-scale visual feature maps from the encoder. ‘SA’ and ‘GAP’ represent spatial attention and global average pooling, respectively. ‘FS’ and ‘MFP’ represent joint-wise feature sampling and multi-plane feature projecting, respectively. ‘TF’ represents a multi-layer transformer. In particular, since our method limits the resolution of feature maps to a maximum of 32×32 during decoding, we only need to adopt the upsampling in the first refinement stage. In addition, for feature maps from the encoder with a resolution greater than 32×32 , we change its resolution by downsampling.

($\mathbf{P}_{left} \in \mathbb{R}^3$ and $\mathbf{P}_{right} \in \mathbb{R}^3$) of the two hands from \mathbf{F}_{left}^{img} and \mathbf{F}_{right}^{img} through Fully Connected (FC) layers, respectively. At the same time, we predict the relative offset $\mathbf{O} \in \mathbb{R}^3$ of the two hands from the features \mathbf{F}_{N-1}^{img} through a 2D average pooling and a FC layer.

3.2. Decoder and Iterative Refinement

Modeling the 3D spatial relationship of the two hands and aligning the estimated mesh with the observed 2D image are two major challenges for interacting hands reconstruction. We address these two problems in the 2D image feature space and 3D joint feature space, respectively, in a decoupled manner. In a single refinement stage, first, we extract joint features from the 2D image feature space according to the 3D-to-2D coordinate relationship. Then, in the 3D joint feature space, we perform intra- and inter-hand information interaction to capture the complex spatial dependencies between two hand joints. Finally, we project the joint-wise features with global context information back to the 2D image space in an unobfuscated way, which provides strong disambiguation clues for local visual features refinement. In particular, we take a total of T refinement stages.

3.2.1 Constructing Joint Feature

For the t -th refinement stage, given the feature map from the previous decoding layer and the skipped feature map \mathbf{F}_{N-t-2}^{img} from the corresponding encoder layer, we concatenate them together and obtain the fused feature map \mathbf{F}^{fusion} by a 1×1 convolution layer. Then, similar to

[43, 47, 50], we obtain joint-wise visual feature $\mathbf{F}_{visual}^{joint} \in \mathbb{R}^{C \times J}$ from \mathbf{F}^{fusion} via a 3D-to-2D coordinate projection and a bilinear interpolation around each projected joint, where J, C represent the joint number and channel dimension of the joint feature. In particular, the projection here is determined by the estimated weak perspective camera, so our method does not require camera intrinsics. In addition, we encode the estimated joint coordinates into coordinate features $\mathbf{F}_{coord}^{joint} \in \mathbb{R}^{C \times J}$ through a FC layer. With the joint-wise visual feature and coordinate features, we can obtain the initial joint features $\mathbf{F}^{joint} = \mathbf{F}_{coord}^{joint} + \mathbf{F}_{visual}^{joint}$. We perform joint feature extraction for two hands independently. In particular, we use the predicted relative offset \mathbf{O} to move the left-hand and right-hand coordinates in the same 3D space.

3.2.2 Modeling Spatial Relationship in 3D Space

For the 3D spatial relationships, our method mainly focuses on two parts, one is the joint dependencies of a single hand, and the other is the spatial context relationships between two hands. First, there are explicit dependencies between the joints of a single hand. For example, when a joint lacks explicit visual cues due to occlusion, we can infer its location based on its related joints such as its parent and child joints. Therefore, we utilize a GCN [52] to perform intra-information interaction between the joint nodes of a single hand based on the skeletal structure. Meanwhile, for the tightly interacting hands, there are more complex and flexible spatial relationships between the joints of the two

hands. Therefore, we adopt a multi-layer transformer [53] to model the relationship between two-hand joints. By using the GCN and the transformer for information interaction, we can obtain enhanced joint features $\tilde{\mathbf{F}}^{joint} \in \mathbb{R}^{C \times J}$ with global information, which are used for MANO parameter prediction and subsequent visual feature enhancement.

Joint nodes have clear semantics, which can take advantage of hand bone structure during interaction and reduces the optimization difficulty of the network. Compared with using redundant nodes to model the two-hand relationship [17], our method can avoid the extra node-to-joint assignment. Compared with performing information interaction between the mesh vertices of two hands [23], our method is computationally efficient and can avoid overfitting.

3.2.3 Enhancing Visual Feature in 2D Space

Benefiting from the local receptive field mechanism and intrinsic inductive bias, 2D convolution can capture local structures efficiently and effectively. However, convolution operations are difficult to model long-range relationships, even when stacking multiple convolutional layers [28]. Therefore, 2D visual features are susceptible to self-occlusion or self-similar appearance interference. To alleviate this problem, we project joint features with global information back to 2D image features. In particular, in order to prevent feature confusion when different joint features are projected back to the same or near pixel positions, we propose a Multi-plane Feature Projecting (MFP). Specifically, we independently project each joint feature to a feature map $\mathbf{F}_j^{proj} \in \mathbb{R}^{J \times H \times W}$ and then concatenate $2J$ feature maps as the final projected feature map $\mathbf{F}^{proj} \in \mathbb{R}^{(2J \times C) \times H \times W}$. Previous work [23, 43, 47, 50] focusing on mesh-image alignment only extracts mesh vertex features unidirectionally from 2D image features and performs refinement in 3D mesh space. These methods do not enhance visual features and ignore the role of convolution operations for pixel-level refinement. In contrast, our method models the dependencies between joints in 3D feature space and then enhances the visual feature map by joint features with global properties.

3.3. Loss Functions

The loss function consists of three parts, including a MANO loss, a relative offset loss, and a pixel-wise loss.

MANO Loss. We supervise the hand joints and meshes predicted by the network. Similar to previous methods [23], we supervise root-relative 3D joint coordinates \mathbf{J}^{3D} , 2D joint coordinates \mathbf{J}^{2D} , 3D coordinates of mesh vertices

\mathbf{V}^{3D} , and 2D coordinates of mesh vertices \mathbf{V}^{2D} as follows:

$$L_{joint} = \sum_{i=0}^{T-1} \sum_{j=0}^{J-1} L1(\mathbf{J}_{i,j}^{3D}, \mathbf{J}_{i,j}^{3D,gt}) + L1(\mathbf{J}_{i,j}^{2D}, \mathbf{J}_{i,j}^{2D,gt}), \quad (3)$$

$$L_{mesh} = \sum_{i=0}^{T-1} \sum_{j=0}^{V-1} L1(\mathbf{V}_{i,j}^{3D}, \mathbf{V}_{i,j}^{3D,gt}) + L1(\mathbf{V}_{i,j}^{2D}, \mathbf{V}_{i,j}^{2D,gt}), \quad (4)$$

where $L1$ represents the smooth L1 loss [15, 16, 37]; T, J, V represents the number of iterative refinements, the number of joints and the number of mesh vertices, respectively. Besides, similar to previous methods [23, 31, 43, 47], we also adopt a normal consistency loss and an edge length consistency to maintain the smoothness of the estimated mesh.

Relative Offset Loss. Accurately estimating the offset between the two hands is important for modeling the spatial relationship of the hands. However, when the distance between the hands is very far, it is difficult to make accurate predictions relying on the cropped image. Indiscriminately predicting the relative offset of the two hands may cause instability in network training. Therefore, we only supervise the hand offset within a certain range.

$$L_{offset} = \begin{cases} L1(\mathbf{O}, \mathbf{O}^{gt}) & \text{if } d < 150 \\ 0 & \text{otherwise.} \end{cases}$$

Here d refers to the 3D Euclidean distance (mm) between the root joints of the two hands.

Pixel-wise Loss. Similar to [50], we utilize auxiliary tasks for pixel-level supervision, enhancing the reliability of visual features. Specifically, we predict two-hand segmentation and dense correspondence maps [23, 35, 46] and supervise them with mean square error (MSE) loss.

4. Experiment

4.1. Implementation Details

We train and evaluate our method on a single server with an NVIDIA A100 Tensor Core GPU. The network is implemented within PyTorch. We train our network using the AdamW [27] optimizer with an initial learning rate of $3e-4$ and a cosine decay learning rate schedule [26]. The whole training process takes 50 epochs with a batch size of 64. We perform data augmentation including random rotation, random scaling, random translation, random horizontal flipping and motion blur. We crop out the hand region based on the 2D coordinates of the hand vertices and resize it to 256×256 . More details about network structure and training details are provided in the supplementary material.

4.2. Datasets

InterHand2.6M. We majorly conduct experiments on InterHand2.6M [33], which provides multi-view RGB images with two-hand mesh and joint 3D annotation. Instead

ID	AM	DRO	IR	GCN	TF	SFP	MHP	MFP	MPJPE	MPVPE
0									8.95	9.17
1	✓								8.87	9.10
2	✓	✓							8.79	9.01
3	✓	✓	✓						8.11	8.36
4				✓					7.86	8.08
5	ALL				✓				7.96	8.19
6				✓	✓				7.74	8.19
7						✓			7.67	7.91
8	ALL			ALL			✓		7.65	7.87
9								✓	7.59	7.80

Table 1. We report the MPJPE (mm) and MPVPE (mm) on Inter-Hand2.6M [33]. ‘AM’ represents using the attention map to split features of the left and right hands. ‘DRO’ represents the distance-aware relative offset loss. ‘IR’ stands for the iterative refinement process from 2D to 3D. ‘SFP’ and ‘MHP’ represent the single-plane feature projection and the multi-plane heatmap projection.

of using multi-view information, we treat all images as single-view images. This dataset is very challenging, it contains complex two-hand interaction poses and covers large-scale perspective changes. Following the practice of [23], we use the 5 FPS version of the released data and only use the interacting two-hand data. Specifically, it consists of 366K training images and 261K testing images.

In-the-wild Datasets. We conduct qualitative experiments on RGB2Hands dataset [46], EgoHands dataset [4], 100DOH dataset [39] and the dataset proposed by Tzionas et al. [45]. These datasets have complex interacting hand samples, diverse backgrounds, realistic lighting conditions and varying image quality, which can provide a comprehensive evaluation of the generalization ability of our approach.

4.3. Evaluation Metrics

Similar to previous methods, we adopt Mean Per Joint Position Error (MPJPE) and Mean Per Vertex Position Error (MPVPE) to measure the accuracy of the pose and shape of the estimated hand meshes. For a fair comparison, we follow the previous work [23, 49] where we perform root joint alignment and scaling according to the ground-truth bone length when evaluating. In particular, in qualitative experiments, we do not perform root joint alignment and scaling. In addition, we also report the Percentage of Correct Key-points (PCK) and Area Under the Curve (AUC) between 0 and 50 millimeters.

4.4. Ablation Study

Basic Network. In this section, we experiment with different ways of predicting initial MANO parameters. Here, our network does not adopt iterative refinements or decoders. As shown in Table 1, the basic method (ID 0) regresses the two-hands MANO parameters and the relative offset directly from the shared global features, which per-

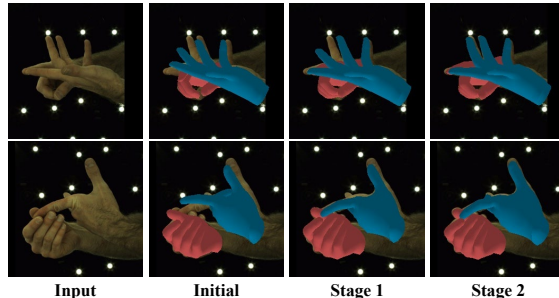


Figure 3. From left to right, we show that the initial hand meshes are gradually corrected. A more accurate spatial relationship modeling can provide stronger disambiguation cues for 2D feature refinement in 2D visual space; better 2D visual features help to construct more representative joint nodes in 3D joint space.

forms poorly. Explicitly separating the two-hand features using an attention map (ID 1) can improve the estimation accuracy of both joints and meshes. Finally, supervising the offset estimation according to 3D Euclidean distance (ID 2) can further improve the performance of the hand reconstruction. In subsequent experiments, by default, we adopt the attention mechanism and distance-aware relative displacement loss. At the same time, in subsequent experiments, we adopt two refinement stages.

Modeling Spatial Relationships In this section, we evaluate the impact of modeling intra- and inter-hand relationships on performance. Compared with not modeling any spatial relationship (ID 3), either using GCN (ID 4) for information interaction between single-hand joints or using a transformer (ID 5) for spatial relationships modeling between two-hand joints can bring a significant performance improvement. Furthermore, using GCN and transformer at the same time (ID 6) can achieve the best performance.

Joint Feature Projection Joint features have global information and thus can provide strong disambiguation cues for local visual features. First, if all joint features are projected into a single plane (ID 7), the features of different joints will be confused, so the performance also drops to a certain extent compared with ID9. Converting the joint coordinates into multiple heatmaps (ID 8) avoids the confusion of different joints, but the information passed to the visual features is limited (only position information), so the performance is not good enough. Multi-plane projection (ID 9) not only avoids feature confusion but also preserves the information of node features well, which achieves the best performance.

Iterative Refinement In this section, we explore the effect of the number of refinement stages on the performance. With one, two, and three refinement stages, MPJPE can reach 7.97 mm, 7.59 mm, and 7.52 mm, respectively, which are about 9.3%, 13.7%, and 14.4% higher than the initial estimation. A better balance of speed and accuracy can be

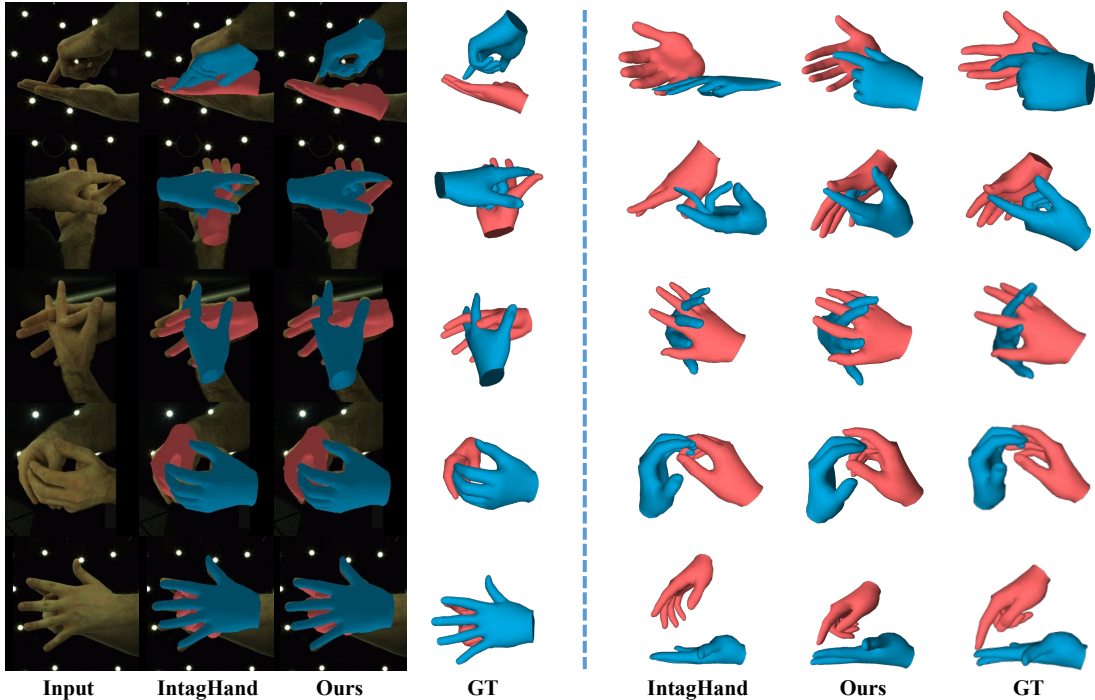


Figure 4. Qualitative results of IntagHand [23] and our method on InterHand2.6M [33] test dataset. Left: frontal view to evaluate the alignment accuracy; Right: another view to observe the plausibility of the estimated two hand meshes.

Method	MPJPE	MPVPE
Zimmermann et al. [55]	36.36	-
Zhou et al. [54]	23.48	23.89
Boukhayma et al. [5]	16.93	17.98
Spurr et al. [42]	15.40	-
InterNet [33]	16.00	
InterShape [49]	13.48	13.95
IntagHand [23]	8.79	9.03
Ours	7.52	7.73

Table 2. We report MPJPE (mm) and MPVPE (mm) on InterHand2.6M [33].

achieved with two-stage refinement (31 FPS), while higher performance can be achieved with three-stage refinement (23 FPS). As shown in Fig 3, our method can effectively correct initial estimates with misaligned meshes or wrong spatial relationships between hands.

4.5. Comparisons with State-of-the-arts

When comparing with SOTA methods, we adopt three refinement stages. We compare our method with single-hand reconstruction methods [5,42,54,55] and two-hand reconstruction methods [23,33,49]. Single-hand reconstruction methods use the ground-truth bounding box to crop the single hand from the input image and predict the two

hands separately. For two-hand reconstruction methods, we mainly compare our method with InterNet [33], InterShape [49] and IntagHand [23]. In particular, IntagHand proposes a dense attention mechanism that greatly improves the accuracy and generalization of interacting two-hand reconstruction. As shown in Table 2, our method significantly outperforms all previous single-hand reconstruction and two-hand reconstruction methods. In particular, compared with SOTA two-hand estimation method IntagHand [23], our method improves by 14.45% (7.52 mm vs. 8.79 mm) and 14.40% (7.73 mm vs. 9.03 mm) in MPJPE and MPVPE. Meanwhile, as shown in Fig. 6, our method outperforms the previous methods at almost all error thresholds.

4.6. Qualitative Results

We present the qualitative results of our method on the Interhand2.6M in Fig. 4. Compared with IntagHand [23], our method can avoid the collapse of the estimated mesh (row 1, row 2); also without a collision constraint, our method can better avoid unreasonable intersections between hands (row 3, row 4). This shows that the joint-based information interaction can help our model capture the spatial relationship between the joints. Meanwhile, our method achieves better mesh-image alignment (row 2, row 3). In particular, when a hand is almost completely occluded (row 5), our method can also infer the pose of the occluded hand



Figure 5. Qualitative results on in-the-wild images. Each row from top to bottom corresponds to RGB2Hands dataset [46], the dataset proposed by Tzionas et al. [45], EgoHands dataset [4] and 100DOH dataset [39]. In each part, the left is the input image, the middle is the result of IntagHand [23], and the right is the result predicted by our method.

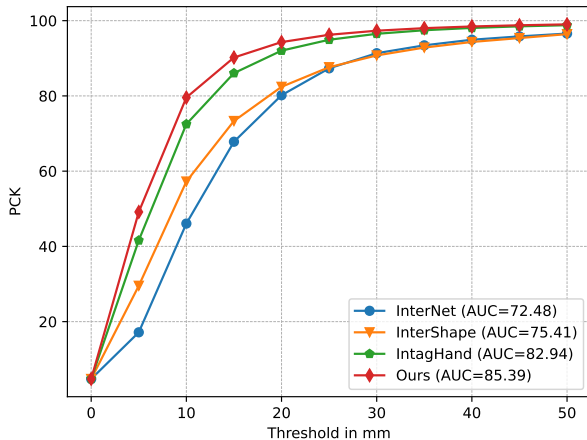


Figure 6. Comparison with SOTA methods on InterHand2.6M [33]. Results of SOTA methods are taken from [23].

based on fine-grained visual cues and global information.

Similar to [23], we also demonstrate the generalization ability of our method on in-the-wild images. It is worth mentioning that we only use InterHand2.6M for training without any additional pre-training on synthetic hand datasets or fine-tuning on other hand datasets. As shown in Fig. 5, our method has a strong generalization ability for different viewpoints such as third or egocentric viewpoints. At the same time, as shown in the third and the last row, our method is robust to different backgrounds and lighting conditions. Since our method is able to enhance visual features with global information, our method is also

relatively robust to object perturbations. In particular, compared with IntagHand [23], which has strong generalization ability, our method also shows obvious advantages, especially in that our method can better maintain hand 3D structure. We present more qualitative results and live demos in the supplementary material.

5. Conclusion

In this paper, we propose a decoupled iterative refinement framework to reconstruct interacting hands from a single RGB image. In order to efficiently model the spatial dependencies between the two hands, we adopt the GCN and the transformer to perform intra- and inter-hand information interaction in the 3D joint feature space. To achieve better alignment of the estimated mesh and observed images, we project the joint features with global information into the visual feature space in a confusion-free manner, which provides strong disambiguation cues for visual features, alleviating self-occlusion and self-similarity problems. Quantitative experiments on InterHand2.6M show that our method outperforms the previous SOTA by a large margin. Meanwhile, experiments on in-the-wild images demonstrate that our method has a strong generalization ability.

Limitation. Our method does not explicitly model collisions between hands, so even with the intra- and inter-hand relationships modeling, intersections between hands still occur, in some cases. Besides, our method does not fully utilize the estimated 3D mesh information. 3D mesh information is helpful for a fine-grained understanding of the relationship between hands.

Supplementary Materials

In the supplemental material, we provide:

- more details of network structure and computational requirements in Sec. A,
- the details of mesh smooth loss in Sec. B,
- more quantitative results in Sec. C,
- more ablation experiments in Sec. D,
- qualitative results in real scenarios and failure examples in Sec. E,

Note that all the notation and abbreviations here are consistent with the main manuscript.

A. Details of Network Structure and Computational Requirements

In this section, we introduce the structure details of the feature fusion layers, the Graph Convolutional Network (CCN) and the transformers. First, we use a residual convolutional module as the stacked hourglass network to fuse the feature maps from the encoder and previous decoding layer. Meanwhile, we use a residual convolution module to enhance the fused visual feature map with projected features. In particular, we set the number of channels of fused visual features and enhanced visual features to 256. We adopt a 4-layer semantic GCN [52] to perform information interaction between the single-hand joints, where the number of channels of joint features is 128. We adopt a 4-layer transformer [53] for information interaction between two-hand joints, in which we add spatial position encoding to the input joint features.

With a single GPU (NVIDIA A100) and a batch size of 64, for the network with two refinement stages, the training time is 39.8h, the memory usage is 22.1G, the FLOPs is 30.8G, and the model parameters are 55.1M. For the network with three refinement stages, the training time is 50.6h, the memory usage is 27.3G, the FLOPs is 46.0G, and the model parameters are 68.6M.

B. Mesh Smooth Loss

Following previous methods [23, 31, 47], we use mesh smooth loss to maintain the estimated mesh geometry reasonable, including a normal consistency loss L_{norm} and edge length consistency loss L_{edge} . L_{norm} is defined as follows:

$$L_{norm} = \sum_f \sum_{\{i,j\} \subset f} \left\| \left\langle \mathbf{e}_{ij}, \mathbf{n}_f^{gt} \right\rangle \right\|_1, \quad (5)$$

where f and \mathbf{n}_f indicate a face of the hand mesh and the unit normal vector of face f , respectively. \mathbf{e}_{ij} indicates an edge of the face f . $\langle \cdot, \cdot \rangle$ is the inner product of two vectors.

L_{edge} is defined as follows:

$$L_{edge} = \sum_f \sum_{\{i,j\} \subset f} \left\| \left\| \mathbf{e}_{ij} \right\|_2, \left\| \mathbf{e}_{ij}^{gt} \right\|_2 \right\|_1. \quad (6)$$

L_{edge} constrains each edge of the predicted mesh to have the same edge length as the ground truth.

	MPJPE	MPVPE
IntagHand [49]	10.66	11.50
IntagHand* [49]	10.03	10.64
Ours	9.00	9.70

Table 3. Quantitative results on Tzionas et al. [45]. We report the MPJPE (mm) and MPVPE (mm). * represents using extra synthetic data for training to improve generalization.

C. More Quantitative Results

In the dataset proposed by Tzionas et al. [45], we selected the sequence containing two hands for quantitative experiments. In particular, we only use this dataset for testing and all models are trained using the InterHand2.6M [33]. As shown in Table 3, our method outperforms IntagHand by a large margin on [45]. Even compared to IntagHand with additional synthetic data, our method has significant advantages, which further demonstrates the superior generalization ability of our method.

D. Ablation Study

We tried multiple practices to improve the performance of the baseline network, including: adopting larger learning rate ($\uparrow 0.4\text{mm}$), adopting SmoothL1 loss instead of L1 loss ($\uparrow 0.1\text{mm}$), predicting MANO parameters instead of joint coordinates ($\uparrow 0.2\text{mm}$), adopting motion blur for data augmentation ($\uparrow 0.1\text{mm}$), etc. If these components are removed, the MPJPE is drop to 9.94mm. It is worth mentioning that since our network is relatively easy to optimize, some practices can achieve obvious results, such as using larger learning rates and adopting motion blur for data augmentation.

In Fig. 7, we show the effect of discarding Multi-Plane Feature Projections (MFP). First, we observe that adopting MFP can alleviate the ambiguity caused by the self-similarity between hands (row1, row2), which indicates that the projected two-hand information provides strong disambiguation cues for local visual features. Second, when there is severe self-occlusion between hands, the projected information can enhance the local visual feature of unobservable regions, significantly improving the robustness of the estimation for the occluded hand (row3, row4). We also observe that adopting MFP can help the network to focus on

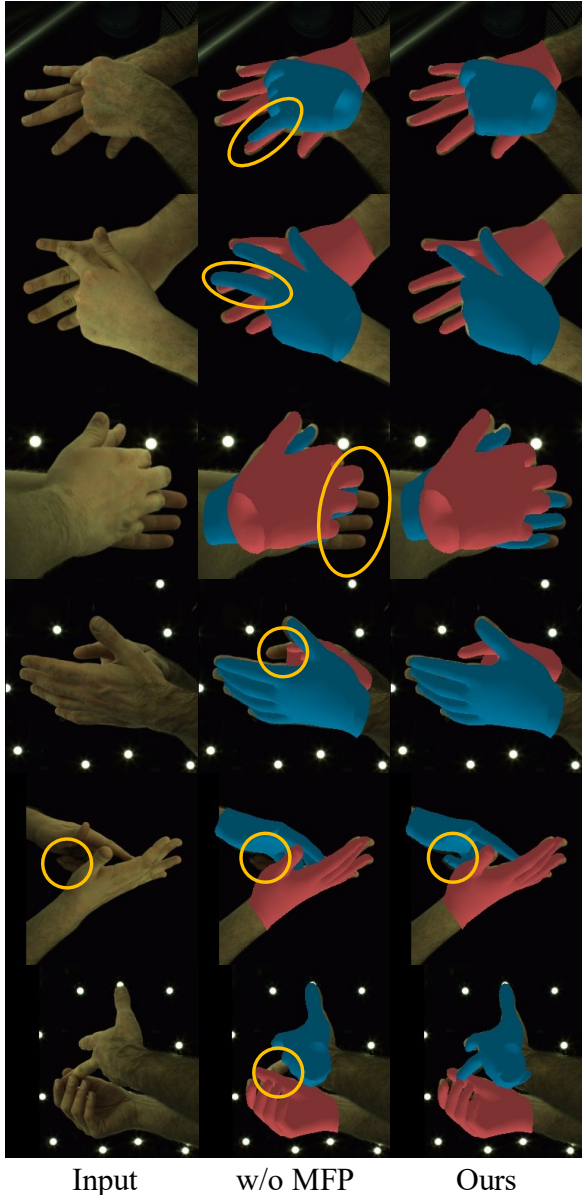


Figure 7. Qualitative ablation study on InterHand2.6M [33]. ‘w/o MFP’ means removing the MFP process from our full model. We highlight the region where the reconstruction is wrong with a yellow circle.

some areas that are easily ignored, such as dark regions and blurred regions (row5, row6).

In Fig. 9, we show the importance of Spatial Relationship modeling (SR) between hands, including the GCN and the transformer. Different from the influence of discarding MFP, discarding spatial interaction usually does not result in significant changes in the rendered 2D mesh, but tends to cause errors in the spatial relationship of invisible parts. As shown in Fig. 9, on the one hand, abandoning spatial in-

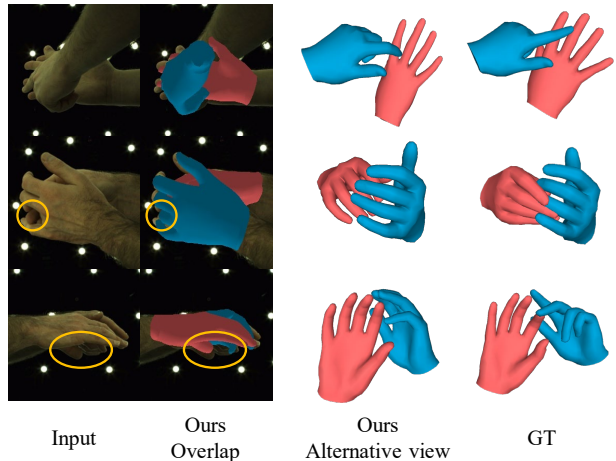


Figure 8. Failure examples on InterHand2.6M [33]. We highlight the region where the reconstruction is wrong with a yellow circle. ‘GT’ means the ground truth.

teractions of the two hands leads to severe intersections and collisions, especially for invisible parts (row1, row2, row3). On the other hand, for the samples with visible interaction regions but complex interaction pose, abandoning two-hand information interaction also leads to the wrong spatial relationship between interacting joints (row4).

E. Qualitative Results

As shown in Fig. 10, we experiment on five subjects in real scenarios. The five subjects have different hand shapes and hand poses. First, our method is able to generate relatively accurate mesh-image alignments for unseen subjects. Second, our method can also perform reasonable reconstructions for some unseen complex interacting poses. Overall, our method achieves efficient pixel-level alignment and 3D spatial relationship modeling thanks to the decoupled design of 2D visual feature space and 3D pose feature space. At the same time, sparse and compact node-level information interaction avoids overfitting and achieves strong generalization ability.

We also show some failure examples. As shown in Fig. 8, for cases with severe self-occlusion and fine-grained interactions (row1), our method does not achieve accurate mesh-image alignment and has a wrong understanding of the two-hand relationship. Second, for examples with severe self-occlusion, when the target joint has few observable pixels (row2) or the observable region is dark (row3), our method cannot reconstruct the corresponding region accurately. In conclusion, our method may fail when multiple conditions such as self-occlusion, tight interaction, blurring or shadowing occur simultaneously or in combination.

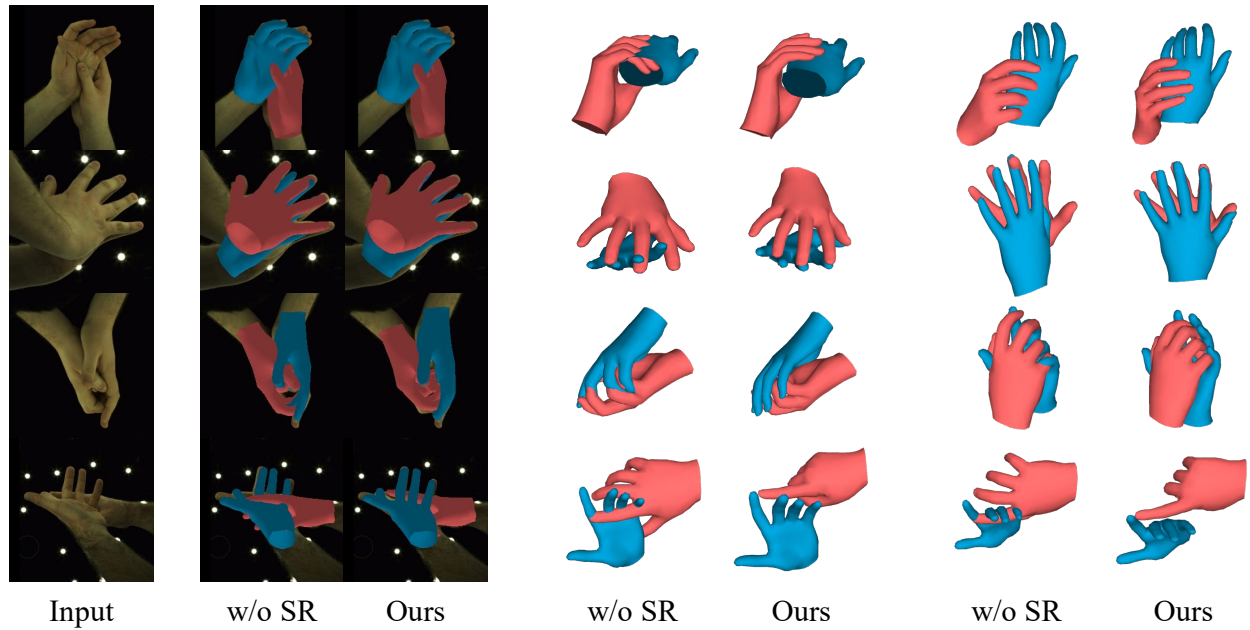


Figure 9. Qualitative ablation study on InterHand2.6M [33]. ‘w/o SR’ means removing the GCN and the transformer from our full model. In this figure, in addition to the mesh that overlaps the input image, we also show the estimated two-hand mesh from two different viewpoints.

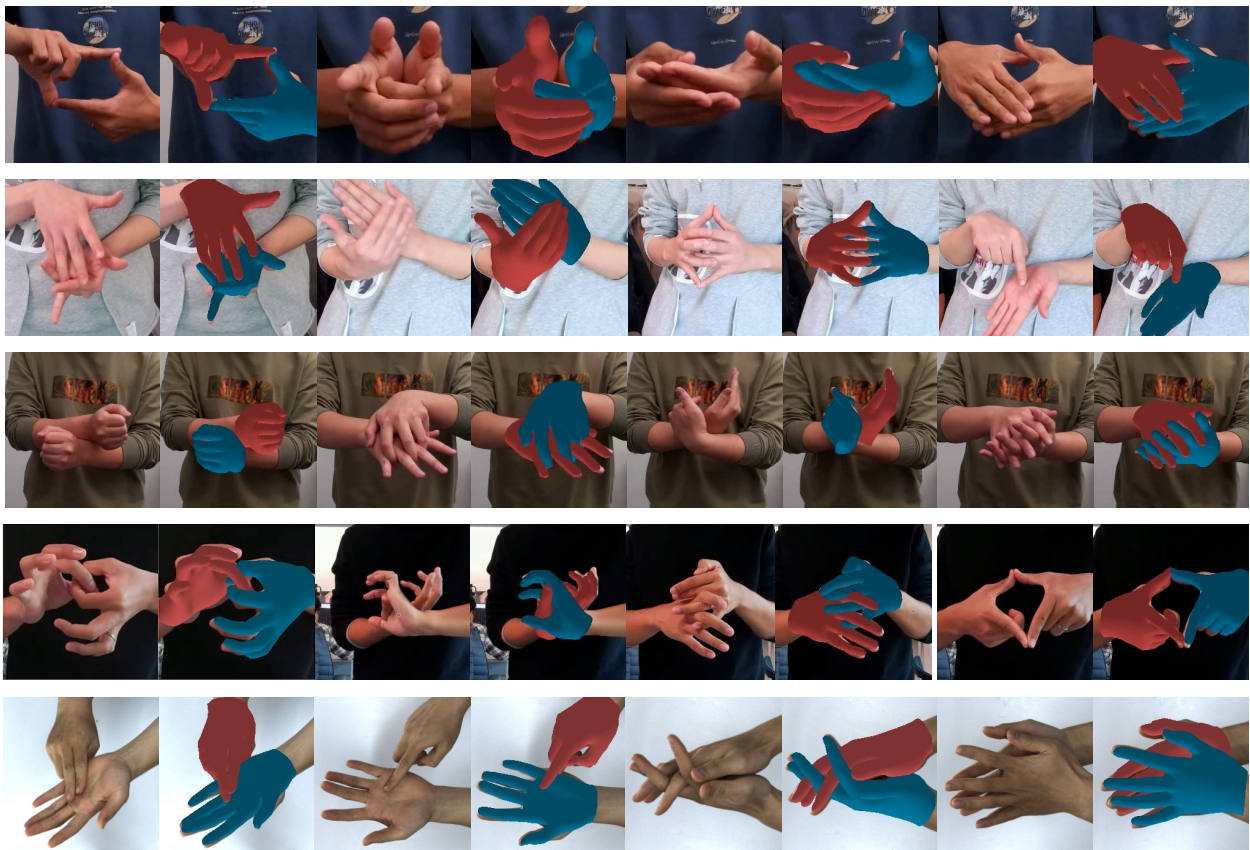


Figure 10. Two-hand reconstruction results in real scenarios on different subjects with different hand shapes and hand poses.

References

- [1] Seungryul Baek, Kwang In Kim, and Tae-Kyun Kim. Pushing the envelope for rgb-based dense 3d hand pose estimation via neural rendering. In *CVPR*, pages 1067–1076, 2019. 1
- [2] Seungryul Baek, Kwang In Kim, and Tae-Kyun Kim. Weakly-supervised domain adaptation via gan and mesh model for estimating 3d hand poses interacting objects. In *CVPR*, pages 6121–6131, 2020. 1
- [3] Luca Ballan, Aparna Taneja, Jürgen Gall, Luc Van Gool, and Marc Pollefeys. Motion capture of hands in action using discriminative salient points. In *ECCV*, pages 640–653. Springer, 2012. 1, 2
- [4] Sven Bambach, Stefan Lee, David J Crandall, and Chen Yu. Lending a hand: Detecting hands and recognizing activities in complex egocentric interactions. In *ICCV*, pages 1949–1957, 2015. 2, 6, 8
- [5] Adnane Boukhayma, Rodrigo de Bem, and Philip HS Torr. 3d hand shape and pose from images in the wild. In *CVPR*, pages 10843–10852, 2019. 1, 2, 7
- [6] Yujun Cai, Lihao Ge, Jianfei Cai, and Junsong Yuan. Weakly-supervised 3d hand pose estimation from monocular rgb images. In *ECCV*, pages 666–682, 2018. 1, 2
- [7] Ping Chen, Yujin Chen, Dong Yang, Fangyin Wu, Qin Li, Qingpei Xia, and Yong Tan. I2uv-handnet: Image-to-uv prediction network for accurate and high-fidelity 3d hand mesh modeling. In *ICCV*, pages 12929–12938, 2021. 1
- [8] Xingyu Chen, Yufeng Liu, Yajiao Dong, Xiong Zhang, Chongyang Ma, Yanmin Xiong, Yuan Zhang, and Xiaoyan Guo. Mobrecon: Mobile-friendly hand mesh reconstruction from monocular image. In *CVPR*, pages 20544–20554, 2022. 1
- [9] Xingyu Chen, Yufeng Liu, Chongyang Ma, Jianlong Chang, Huayan Wang, Tian Chen, Xiaoyan Guo, Pengfei Wan, and Wen Zheng. Camera-space hand mesh recovery via semantic aggregation and adaptive 2d-1d registration. In *CVPR*, pages 13274–13283, 2021. 1
- [10] Junhyeong Cho, Kim Youwang, and Tae-Hyun Oh. Cross-attention of disentangled modalities for 3d human mesh recovery with transformers. In *ECCV*, pages 342–359. Springer, 2022. 2
- [11] Hongsuk Choi, Gyeongsik Moon, and Kyoung Mu Lee. Pose2mesh: Graph convolutional network for 3d human pose and mesh recovery from a 2d human pose. In *ECCV*, pages 769–787. Springer, 2020. 2
- [12] Jia Deng, Wei Dong, Richard Socher, Li-Jia Li, Kai Li, and Li Fei-Fei. Imagenet: A large-scale hierarchical image database. In *CVPR*, pages 248–255. Ieee, 2009. 3
- [13] Zicong Fan, Adrian Spurr, Muhammed Kocabas, Siyu Tang, Michael J Black, and Otmar Hilliges. Learning to disambiguate strongly interacting hands via probabilistic per-pixel part segmentation. In *3DV*, pages 1–10. IEEE, 2021. 2, 3
- [14] Lihao Ge, Zhou Ren, Yuncheng Li, Zehao Xue, Yingying Wang, Jianfei Cai, and Junsong Yuan. 3d hand shape and pose estimation from a single rgb image. In *CVPR*, pages 10833–10842, 2019. 2, 3
- [15] Ross Girshick. Fast r-cnn. In *ICCV*, pages 1440–1448, 2015. 5
- [16] Hengkai Guo, Guijin Wang, Xinghao Chen, Cairong Zhang, Fei Qiao, and Huazhong Yang. Region ensemble network: Improving convolutional network for hand pose estimation. In *ICIP*, pages 4512–4516. IEEE, 2017. 5
- [17] Shreyas Hampali, Sayan Deb Sarkar, Mahdi Rad, and Vincent Lepetit. Keypoint transformer: Solving joint identification in challenging hands and object interactions for accurate 3d pose estimation. In *CVPR*, pages 11090–11100, 2022. 2, 3, 5
- [18] Kaiming He, Xiangyu Zhang, Shaoqing Ren, and Jian Sun. Deep residual learning for image recognition. In *CVPR*, June 2016. 3
- [19] Umar Iqbal, Pavlo Molchanov, Thomas Breuel, Jürgen Gall, and Jan Kautz. Hand pose estimation via latent 2.5 d heatmap regression. In *ECCV*, pages 118–134, 2018. 1, 2
- [20] Dong Uk Kim, Kwang In Kim, and Seungryul Baek. End-to-end detection and pose estimation of two interacting hands. In *CVPR*, pages 11189–11198, 2021. 2, 3
- [21] Dominik Kulon, Riza Alp Guler, Iasonas Kokkinos, Michael M Bronstein, and Stefanos Zafeiriou. Weakly-supervised mesh-convolutional hand reconstruction in the wild. In *CVPR*, pages 4990–5000, 2020. 1, 2, 3
- [22] Nikolaos Kyriazis and Antonis Argyros. Scalable 3d tracking of multiple interacting objects. In *CVPR*, pages 3430–3437, 2014. 1, 2
- [23] Mengcheng Li, Liang An, Hongwen Zhang, Lianpeng Wu, Feng Chen, Tao Yu, and Yebin Liu. Interacting attention graph for single image two-hand reconstruction. In *CVPR*, pages 2761–2770, 2022. 1, 2, 3, 5, 6, 7, 8, 9
- [24] Kevin Lin, Lijuan Wang, and Zicheng Liu. End-to-end human pose and mesh reconstruction with transformers. In *CVPR*, pages 1954–1963, June 2021. 2
- [25] Kevin Lin, Lijuan Wang, and Zicheng Liu. Mesh graphormer. In *ICCV*, pages 12939–12948, 2021. 2, 3
- [26] Ilya Loshchilov and Frank Hutter. Sgdr: Stochastic gradient descent with warm restarts. *arXiv preprint arXiv:1608.03983*, 2016. 5
- [27] Ilya Loshchilov and Frank Hutter. Decoupled weight decay regularization. *arXiv preprint arXiv:1711.05101*, 2017. 5
- [28] Wenjie Luo, Yujia Li, Raquel Urtasun, and Richard Zemel. Understanding the effective receptive field in deep convolutional neural networks. *NIPS*, 29, 2016. 5
- [29] Hao Meng, Sheng Jin, Wentao Liu, Chen Qian, Mengxiang Lin, Wanli Ouyang, and Ping Luo. 3d interacting hand pose estimation by hand de-occlusion and removal. In *ECCV*, 2022. 3
- [30] Gyeongsik Moon, Hongsuk Choi, and Kyoung Mu Lee. Accurate 3d hand pose estimation for whole-body 3d human mesh estimation. In *Proceedings of the IEEE/CVF Conference on Computer Vision and Pattern Recognition (CVPR) Workshops*, pages 2308–2317, June 2022. 2
- [31] Gyeongsik Moon and Kyoung Mu Lee. I2l-meshnet: Image-to-lixel prediction network for accurate 3d human pose and mesh estimation from a single rgb image. In *ECCV*, pages 752–768. Springer, 2020. 1, 5, 9
- [32] Gyeongsik Moon, Takaaki Shiratori, and Kyoung Mu Lee. Deephandmesh: A weakly-supervised deep encoder-decoder

- framework for high-fidelity hand mesh modeling. In *ECCV*, pages 440–455. Springer, 2020. [1](#)
- [33] Gyeongsik Moon, Shoou-I Yu, He Wen, Takaaki Shiratori, and Kyoung Mu Lee. Interhand2.6m: A dataset and baseline for 3d interacting hand pose estimation from a single rgb image. In *ECCV*, pages 548–564. Springer, 2020. [3](#), [5](#), [6](#), [7](#), [8](#), [9](#), [10](#), [11](#)
- [34] Franziska Mueller, Florian Bernard, Oleksandr Sotnychenko, Dushyant Mehta, Srinath Sridhar, Dan Casas, and Christian Theobalt. Gnerated hands for real-time 3d hand tracking from monocular rgb. In *CVPR*, pages 49–59, 2018. [1](#)
- [35] Franziska Mueller, Micah Davis, Florian Bernard, Oleksandr Sotnychenko, Mical Verschoor, Miguel A Otaduy, Dan Casas, and Christian Theobalt. Real-time pose and shape reconstruction of two interacting hands with a single depth camera. *TOG*, 38(4):1–13, 2019. [1](#), [3](#), [5](#)
- [36] Iasonas Oikonomidis, Nikolaos Kyriazis, and Antonis A Argyros. Tracking the articulated motion of two strongly interacting hands. In *CVPR*, pages 1862–1869. IEEE, 2012. [1](#), [2](#)
- [37] Pengfei Ren, Haifeng Sun, Qi Qi, Jingyu Wang, and Weiting Huang. Srn: Stacked regression network for real-time 3d hand pose estimation. In *BMVC*, page 112, 2019. [5](#)
- [38] Javier Romero, Dimitrios Tzionas, and Michael J. Black. Embodied hands: Modeling and capturing hands and bodies together. *TOG*, 36(6), 2017. [3](#)
- [39] Dandan Shan, Jiaqi Geng, Michelle Shu, and David F Fouhey. Understanding human hands in contact at internet scale. In *CVPR*, pages 9869–9878, 2020. [2](#), [6](#), [8](#)
- [40] Breannan Smith, Chenglei Wu, He Wen, Patrick Peluse, Yaser Sheikh, Jessica K Hodgins, and Takaaki Shiratori. Constraining dense hand surface tracking with elasticity. *TOG*, 39(6):1–14, 2020. [1](#), [3](#)
- [41] Adrian Spurr, Umar Iqbal, Pavlo Molchanov, Otmar Hilliges, and Jan Kautz. Weakly supervised 3d hand pose estimation via biomechanical constraints. In *ECCV*, pages 211–228. Springer, 2020. [1](#)
- [42] Adrian Spurr, Jie Song, Seonwook Park, and Otmar Hilliges. Cross-modal deep variational hand pose estimation. In *CVPR*, pages 89–98, 2018. [2](#), [7](#)
- [43] Xiao Tang, Tianyu Wang, and Chi-Wing Fu. Towards accurate alignment in real-time 3d hand-mesh reconstruction. In *ICCV*, pages 11698–11707, 2021. [2](#), [3](#), [4](#), [5](#)
- [44] Jonathan Taylor, Vladimir Tankovich, Danhang Tang, Cem Keskin, David Kim, Philip Davidson, Adarsh Kowdle, and Shahram Izadi. Articulated distance fields for ultra-fast tracking of hands interacting. *TOG*, 36(6):1–12, 2017. [1](#), [3](#)
- [45] Dimitrios Tzionas, Luca Ballan, Abhilash Srikantha, Pablo Aponte, Marc Pollefeys, and Juergen Gall. Capturing hands in action using discriminative salient points and physics simulation. *IJCV*, 118(2):172–193, 2016. [2](#), [6](#), [8](#), [9](#)
- [46] Jiayi Wang, Franziska Mueller, Florian Bernard, Suzanne Sorli, Oleksandr Sotnychenko, Neng Qian, Miguel A Otaduy, Dan Casas, and Christian Theobalt. Rgb2hands: real-time tracking of 3d hand interactions from monocular rgb video. *TOG*, 39(6):1–16, 2020. [2](#), [3](#), [5](#), [6](#), [8](#)
- [47] Nanyang Wang, Yinda Zhang, Zhuwen Li, Yanwei Fu, Wei Liu, and Yu-Gang Jiang. Pixel2mesh: Generating 3d mesh models from single rgb images. In *ECCV*, pages 52–67, 2018. [3](#), [4](#), [5](#), [9](#)
- [48] Chao Wen, Yinda Zhang, Zhuwen Li, and Yanwei Fu. Pixel2mesh++: Multi-view 3d mesh generation via deformation. In *ICCV*, pages 1042–1051, 2019. [3](#)
- [49] Baowen Zhang, Yangang Wang, Xiaoming Deng, Yinda Zhang, Ping Tan, Cuixia Ma, and Hongan Wang. Interacting two-hand 3d pose and shape reconstruction from single color image. In *CVPR*, pages 11354–11363, 2021. [2](#), [3](#), [6](#), [7](#), [9](#)
- [50] Hongwen Zhang, Yating Tian, Xinchu Zhou, Wanli Ouyang, Yebin Liu, Limin Wang, and Zhenan Sun. Pymaf: 3d human pose and shape regression with pyramidal mesh alignment feedback loop. In *ICCV*, pages 11446–11456, 2021. [2](#), [3](#), [4](#), [5](#)
- [51] Xiong Zhang, Qiang Li, Hong Mo, Wenbo Zhang, and Wen Zheng. End-to-end hand mesh recovery from a monocular rgb image. In *ICCV*, pages 2354–2364, 2019. [1](#), [2](#)
- [52] Long Zhao, Xi Peng, Yu Tian, Mubbasir Kapadia, and Dimitris N Metaxas. Semantic graph convolutional networks for 3d human pose regression. In *CVPR*, pages 3425–3435, 2019. [2](#), [4](#), [9](#)
- [53] Ce Zheng, Sijie Zhu, Matias Mendieta, Taojiannan Yang, Chen Chen, and Zhengming Ding. 3d human pose estimation with spatial and temporal transformers. In *ICCV*, pages 11656–11665, 2021. [2](#), [5](#), [9](#)
- [54] Yuxiao Zhou, Marc Habermann, Weipeng Xu, Ikhsanul Habibie, Christian Theobalt, and Feng Xu. Monocular real-time hand shape and motion capture using multi-modal data. In *CVPR*, pages 5346–5355, 2020. [2](#), [7](#)
- [55] Christian Zimmermann and Thomas Brox. Learning to estimate 3d hand pose from single rgb images. In *ICCV*, pages 4903–4911, 2017. [1](#), [2](#), [7](#)
- [56] Christian Zimmermann, Duygu Ceylan, Jimei Yang, Bryan Russell, Max Argus, and Thomas Brox. Freihand: A dataset for markerless capture of hand pose and shape from single rgb images. In *ICCV*, pages 813–822, 2019. [1](#)